Extinction of solid diffusion flame in microgravity: details of quenching and blowoff processes

Chengyao Li[a], James S. T'ien[a,*], Paul V. Ferkul[b], Sandra L. Olson[c], Michael C. Johnston[c]

[a]*Department of Mechanical and Aerospace Engineering, Case Western Reserve University, Cleveland, OH, USA*
[b]*Universities Space Research Association, NASA Glenn Research Center, Cleveland, OH, USA*
[c] *NASA Glenn Research Center, Cleveland, OH, USA*

Abstract

Long duration microgravity experiments aboard the International Space Station determine diffusion flame extinction limits of PMMA spheres. Upon ignition from an electrically-heated coil, the 4-cm-diameter samples are exposed to forced flows ranging from 0.2 to 80 cm/s and an oxygen ranging from 13 to 28% in one atmosphere total pressure. Extinction is reached as oxygen concentration gradually decreases by natural depletion. Five extinction tests are presented at different flow velocities and oxygen concentrations. Quenching at low velocity is observed with the flame tip shrinking upstream and blowoff is observed when a hole forms in the flame at the forward flow stagnation point. However, these processes are not quasistatic. The quenching motion involves periodic flame tip pulsating toward downstream and shrinking upstream with a continually decreasing flame size at the end of each cycle. In blowoff, the flame base pulsates between the flame hole and the downstream location, although with far fewer cycles compared to quenching. The pulsations appear to be the result of a premixed flame front spreading into a combustible mixture. Two specific cases are discussed. In the first, at very low flow velocity (~ 0.4 cm/s) and elevated oxygen, self-sustained flame tip cyclic pulsations are observed for a lengthy period (~15 minutes). In the second case with a higher flow velocity (50 cm/s), the diffusion flame is stabilized at the shoulder of the spherical sample after local stagnation point blowoff. With steady decrease in ambient oxygen due to depletion, spinning flamelets are formed. The long-duration microgravity environment makes it possible to observe these interesting and detailed extinction processes.

Keywords: Flame quenching; Flame blowoff; Flame pulsation; Low stretch flame; Microgravity

*Corresponding author.

1. Introduction

Extinction of diffusion flames is a classical topic with practical relevance to many combustion systems. Aerodynamic blowoff due to flow residence times can be interpreted using a critical small Damkohler number concept [1,2] and is a flame stabilization problem. Aerodynamic quenching in slow flow (at long residence times) is the consequence of flame heat losses [3]. In slow flows, the combustion intensity is reduced and the ratio of heat loss (by radiation, for example) to heat generation is increased. The resulting reduced flame temperature leads to quenched extinction. Although blowoff experiments are common, aerodynamic quenching studies in an open-air environment (long residence time) are uncommon, especially for solid fuels [4,5]. This is because the magnitude of the flow required for quenching is typically lower than that of the always present buoyancy-induced flow in normal Earth gravity. On Earth, low buoyant stretch stagnation-point flames can only be obtained using very large diameter solid samples [6] or large radius burners [7,8]. To test a sample of a given size in low-speed flow, a microgravity environment is needed. In microgravity, the magnitude of the imposed (forced) flow can be independently controlled.

Microgravity experiments are also important to spacecraft fire safety. Understanding extinction limits of solid materials is important to interpret the results of material screening tests performed on earth [9,10].

For thick solids with large solid-phase thermal response times, long-duration microgravity environments are needed. The present work is a part of the Growth and Extinction Experiment (GEL), which is the first of the five original experiments in the SoFIE (Solid Fuel Ignition and Extinction) project. SoFIE is a NASA Biological and Physical Sciences (BPS) sponsored project on the International Space Station (ISS) on solid combustion [11]. The solid sample used in GEL is a 4-cm diameter PMMA (polymethylmethacrylate) sphere. The experimental findings of both quenching and blowoff processes are reported here, emphasizing the differences of their near-limit behaviors.

2. Experiment setup

The experiment is conducted using the SoFIE insert (main components shown in Fig.1) which is placed inside the Combustion Integrated Rig (CIR) aboard the ISS. CIR is equipped with a power supply, filters, lighting, gas cylinder intakes, radiometers, and oxygen, pressure, velocity and CO, CO_2 sensors. In this paper, oxygen percentage is reported from the sensor located at the flow duct entrance. The SoFIE insert has a square flow duct (13.3 cm x 13.3 cm cross-section and 24.6 cm long). Forced flow ranging from 0.2 - 80 cm/s is generated by two fan banks. A flow sensor at the upstream end of the flow duct provides a flow velocity reading. The spherical PMMA sample (4 cm diameter) used in GEL is supported by a long stainless-steel tube (6.35 mm diameter). Three samples are mounted 120° apart on an index system that can be rotated to install one sample at a time with the flow duct.

Once the astronaut installs the samples and the oxidizer gas cylinders in the ISS, the rest of the experiment is controlled remotely from the NASA Glenn Research Center ISS Payload Operations Center (GIPOC). During the test, one sample is placed along the centerline of flow duct and about 1 cm from the duct exit for ignition. The igniter is an electrically heated coiled wire placed near the upstream stagnation point of the sphere. After ignition, the igniter is retracted. The sample can either stay at this location for the whole test or be translated into the duct.

Four fixed cameras are used for flame visualization. Three Sony FCB-MA130 cameras with a 1400 x 1200 pixel array (named SoFIE Cam1,Cam2, and Cam3) are in orthogonal direction of a 1.4 megapixel Allied Vision GC-1380CH ACME color camera assembly with a 1360 x 1024 pixel array. SoFIE Cam1 views the sample near the ignition location. SoFIE Cam2 and ACME are aligned and view the sample at the location after translating into the duct. SoFIE Cam3 is not activated in the cases presented in this paper.

All the extinction cases in this paper are obtained using a natural and gradual oxygen depletion while the flow speed is held constant. In the sealed CIR chamber (free volume = 85.7 liter), oxygen is slowly consumed. This oxygen depletion method is the least intrusive (i.e., free of external disturbances), which is important both for determining accurate extinction limits and for observing spontaneous cyclical extinction dynamics [12,13,20]. Note that real time oxygen concentration measurement is made at the flow duct entrance upstream of the sample.

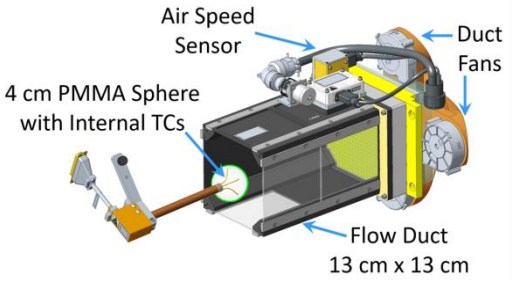

Fig. 1. Diagram of the SoFIE flow duct with a thermocouple-instrumented GEL sphere sample.

The PMMA sphere samples are custom cast with five embedded thermocouples as illustrated in Fig. 1. Three thermocouples are placed along the center line close to the forward stagnation point. They are used to deduce the subsurface temperature gradient, which is a measure of the degree of solid sub-surface heating. More details on the preparation and

fabrication of the samples and the method to compute the temperature gradient can be found in [14,15].

The 4-cm-diameter sphere was selected since it is a thick solid representative of many non-thin materials used in spacecraft. The spherical geometry has a richness of flame physics to study. When placed in an airflow stream, there are several distinct regions around the sphere, exhibiting different fluid mechanics characteristics. In front of the sphere, stagnation point flow develops. Flames in this region are locally one-dimensional when the flame thickness is much smaller than the sphere radius, and experimental results can be compared with one-dimensional models. This is also the flame stabilization region that controls the extinction characteristics of the envelope flame. The existence of the sphere shoulder and wake regions, on the other hand, can reveal additional multi-dimensional features of the extinction processes (to be discussed later). PMMA spheres have also been employed in [16-18].

3. Experimental results

Five tests are presented as listed in Table 1. Cases 1 to 3 are representative of low-flow quenching, high-flow blowoff, and intermediate-flow extinction, respectively. The differences between quenching and blowoff are highlighted in sections 3.1-3.3. In section 3.4 and 3.5, a very low flow test (Case 4) and a higher flow test (Case 5) are shown. These last two tests reveal novel behavior and delineate the prominent features of the solid extinction phenomena.

Table 1
List of 5 test cases: extinction mode, sample location and extinction parameters

Case #	GEL sample #	Extinction mode	Sample location	Flow (cm/s)	Re[a]	Flow strain rate[b] (1/s)	O_2 (%)	p (atm)	Conductive heat loss (W/cm^2)
1	1409B	quenching	inside duct	4.83	128.8	3.63	14.21	1.04	0.36
2	1408A	blowoff	inside duct	34.28	914.1	25.71	14.99	1.06	0.95
3	1402C	intermediate	Inside duct	11.50	306.7	8.63	13.54	1.07	0.37
4	1409C	quenching	duct exit	0.44	11.7	0.33	20.77	1.03	0.17
5	1410C	blowoff	duct exit	49.68	1324.8	37.26	14.37	1.07	not recorded

[a]Reynolds numbers are evaluated at ambient temperature based on sphere diameter.
[b]Stagnation-point flow strain rate $a = 3/2\ U/R$, where U is the flow velocity and R is the sphere radius.

3.1 A quenching sequence

Figure 2 shows images of a representative quenching sequence from Case #1. During the extinction process (500 – 757.55 s), the flow velocity slightly varies between 4.46 – 4.92 cm/s, and oxygen depletes to extinction. There is a gradually increasing trend of the flow sensor reading in this time range. It is a result of flow resistance change, probably related to a slight decrease of chamber pressure during quenching due to the combustion products filtering. Figure 2(a) shows the flame tip is at around 100° (measured from the front stagnation point). This is the furthest downstream that flame reaches as seen in the tracking of tip2 (red color) in Fig. 3. As oxygen slowly depletes, the flame tip slowly shrinks toward upstream (Fig 2(b)). As shown in Fig. 3, the flame tip begins to have small fluctuations later (also illustrated in Fig. 2(c)). The fluctuations have varied amplitudes and time periods. Large amplitude cyclic flame tip pulsation and retreating starts much later at about 744 s. With each pulsation cycle, the flame tip retreats more toward upstream and results in a shorter instant flame length until extinction occurred at 757.55 s.

Figure 3 shows the flame tip tracking. Tracking is based on images in the orthogonal direction of that in Fig. 2. Flame tip position is represented by the angle around the sphere with zero degrees at the forward stagnation point. Positive and negative angles are used to track the left and right tip position. Test telemetries of oxygen, pressure, and flow velocity are also plotted. The inset plot shows the zoom-in of the flame tip pulsations near extinction. Solid lines in the inset plot connect the data points to show pulsations. Black dotted line in the inset plot shows the decreasing trend with time of the lowest point in each cycle of tip2. Extinction occurred when tip2 shrinks past the stagnation region stabilization zone. The asymmetry between the two tips may be due to a slightly unsymmetric ignition or the intrinsic nature of the near-limit flames.

Comparing the diffusion flame CH* luminosity near the stagnation point with the flame pulsation luminosity, the increased intensity of the flame during pulsating downstream seen in Fig. 2(e) suggests that this part is a premixed flame. The broaden flame image toward the back of the sphere suggests a widened reaction zone [19]. The hypothesis is that after flame tip retreat, fuel vapor can form a combustible mixture with varying fuel-air equivalence ratio distribution. The fuel vapor may come from two possible sources: leakage from the opening between the flame tip and the surface and pyrolysis from the newly exposed hot solid. The fact that the pulsating flame tip can reach far downstream to the rear of the sphere beyond the initial diffusion flame tip (see Fig. 3 inset and Fig 2(e)) supports the fuel leakage hypothesis. Additional discussion will be made in Sections 3.4.

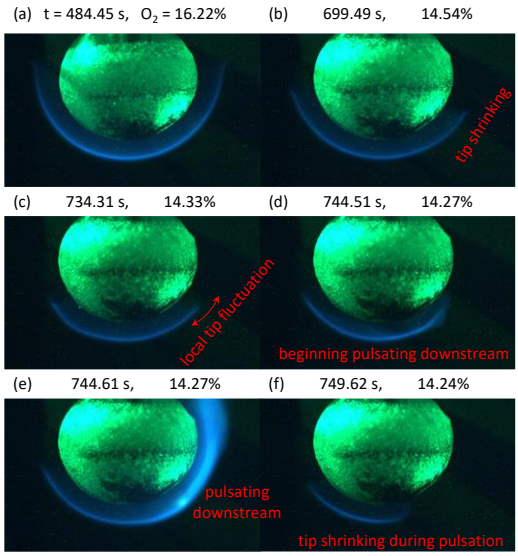

Fig. 2. A representative quenching time sequence for Case #1 from ACME camera (see supplementary video S1 for full video).

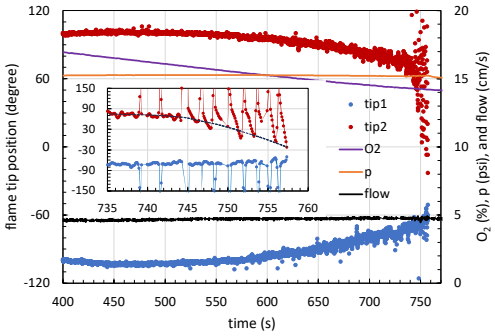

Fig. 3. Flame tip tracking for Case #1 using the SoFIE Cam2. Legend and axes are the same for inset.

There are ten completed flame tip pulsating and retreating cycles before quenching (i.e., flame reaches the back of the sphere) as shown in the inset of Fig. 3. The pulsation to downstream takes more time in the first two cycles but reaches constant 0.4 s period for the remaining. Note that when the net downstream pulsation speed reaches peak, the flame has largest luminosity (Fig. 2(e)), consistent with a previous work on blowoff oscillation over PMMA rods [20]. The downstream pulsation speed is within the range of typical laminar premixed burning velocity. After the flame pulsating downstream and consuming the combustible mixture, the flame tip shrinks. The shrinking time period ranges from 1.5 s to 0.8 s and the shrinking speed is much slower than pulsating downstream. Note that in each cycle, the flame tip shrinks more toward upstream as shown in Fig. 3. So, on the average the flame length is shrinking.

3.2 A blowoff sequence

Figure 4 shows a representative blowoff sequence from Case #2 (34.28 cm/s flow). Figure 4(a) shows that at 200 s, flame is still away from extinction at 16.6% O_2. The sample is located inside the flow duct. The flame tip is slightly directed toward the centerline because of the flow restriction inside the duct. The yellowish flame indicates soot formation. When the ambient oxygen decreases, the flame turns blue.

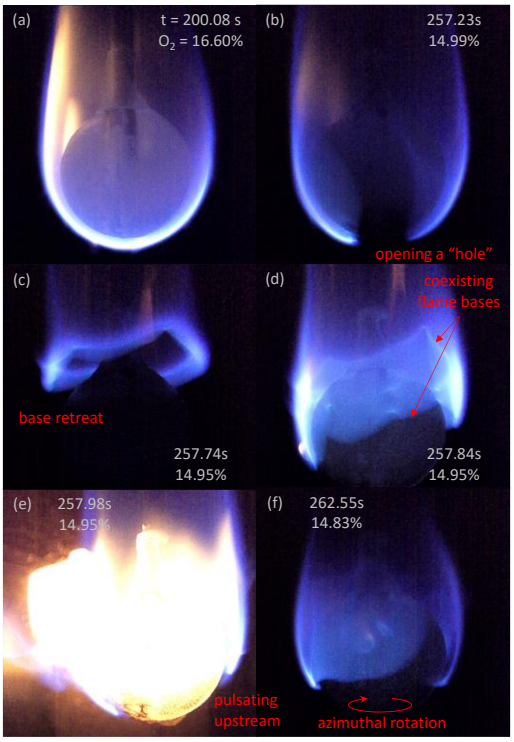

Fig. 4. A representative blowoff case (Case #2) from SoFIE Cam2 (see supplementary video S2 for full video).

Extinction starts with a flame hole at the stagnation point (Fig. 4(b)). This local flame blowoff occurs when oxygen is below the limit (14.99%) for this particular stagnation flow strain rate (25.7 s^{-1}). The flame base then retreats downstream to the near-wake region, where the flow velocity is smaller (Fig. 4(c)). After the flame base retreats, the still hot solid surface continues generating fuel vapor while mixing with incoming oxygen. The flame base then pulsates upstream all the way to the stagnation region (Fig. 4(e)). During the upstream pulsation, the flame base shape is irregular, and part of the base is in the wake region and the other part is in the shoulder region (Fig. 4(d)). In this blowoff case, there are only two flame base pulsation cycles. Flame base travels averaging 5.4 cm in pulsation. The upstream pulsation periods are 0.41 s, and the flame base retreats take 0.21 and 0.31 s. Similar to Case #1, the upstream pulsation

speed is within the typical laminar premixed burning velocity range. After the two pulsation cycles, the flame shows azimuthal spinning (3D instability) for 3.18 s with flame base anchored at the shoulder region of the sphere before complete blowoff extinction.

3.3 Extinction at intermediate flow velocities and flow strain rates

In the previous sections we have shown how different the extinction processes for low-flow quenching and high-flow blowoff are. In quenching, the flame tip shrinks toward the upstream, in blowoff, the flame base retreats toward the downstream. In quenching, the flame tip pulsates while in blowoff, the flame base pulsates. One natural question is how does the flame go to extinction at intermediate flow velocities where the quenching and the blowoff boundaries meet? The meeting point of the two branches has been referred to as the fundamental limit where the oxygen limit is the lowest [3].

We have examined several test results in the intermediate flow range between 9.22 and 11.5 cm/s (strain rates 6.92-8.23 s^{-1}). They all exhibit the same description on the extinction processes as follows. As oxygen is depleted, flame tip shrinks but without any pulsation. Near extinction, the flame base color began to fade (a prelude to local blowoff or hole forming) but the flame goes out normally in one video frame without any base pulsation either. So, the transition from quench to blowoff is smooth along the extinction boundary. Case #3 in Table 1 is a representative intermediate case (see supplementary video S3).

3.4 Self-sustained cyclic flame pulsation

Case #4 is an ultra-low velocity case at relatively high oxygen atmosphere. As shown in Fig. 5(a), the flame tip pulsating downstream starts at 311 s, immediately after the nominal flow velocity is turned down to 0.4 cm/s at 309 s, and lasts until quenching at 1237.88 s, for a total period of 927 s. In contrast, the near-limit pulsation in Case #1 only lasts for 18.84 s. In addition to flame tip position, test telemetries of oxygen, pressure, and flow velocity are also plotted in Fig. 5(a). It shows one side of the flame initiates the cyclic pulsation and the other side starts much later at around 1040 s. When the pulsation starts, oxygen concentration is at 26.25%. It gradually depletes to 20.77% at quenched extinction. During most of the time, the pulsations are under elevated oxygen concentration. If the oxygen were not depleted, the pulsative cycles would have lasted even longer. So, we will refer this case as a "self-sustained" flame pulsation (i.e., limit cycle). During pulsations, though the nominal flow velocity is held constant at 0.2 cm/s (except the 0.4 cm/s set flow in the beginning 10 s), the flow sensor reading ranged from 0.16 to 0.5 cm/s. Similar to Case #1, there is a gradual increase of flow velocity during the quenching process (Fig. 5(a)). Starting at around 880 s, there is also flow velocity oscillations in phase with the flame pulsation. Figure 5(b) shows 10 s of the flame tip tracking and the flow sensor reading near extinction. The flow velocity fluctuation is thought to be the result of flame-flow interaction since the flow is very weak and these large-scale flame pulsations affect the flow resistance in the duct.

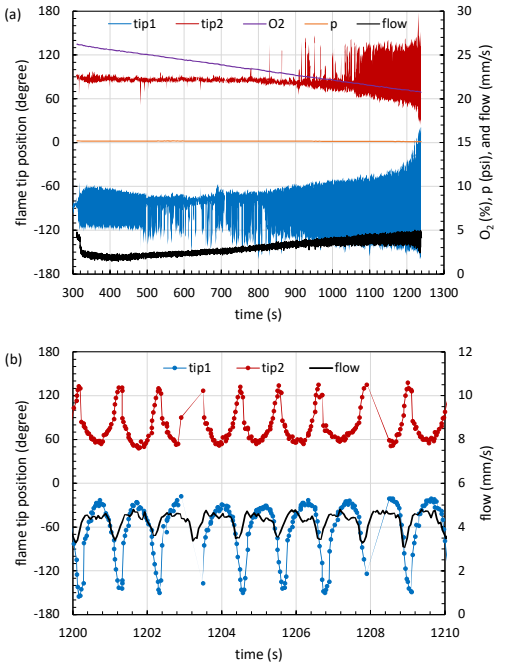

Fig. 5. Flame tip tracking of (a) the whole cyclic pulsation period and (b) 10 s near extinction for Case #4 using SoFIE Cam1.

The 30-fps frame rate gives very good resolution of the flame tracking in Fig. 5(b) within one cycle. The shape of the cycle shows that the flame tip spends much less time at the downstream position than at the upstream position. The trajectory of the tip is not sinusoidal or near-sinusoidal like typical oscillations. This is because the present cycle has two distinct time scales: the propagation time in a fuel-air mixture and the preparation time to form a new mixture after the flame passage. Figure 5(b) shows that the preparation time is the longer of the two although they are still within the same order of magnitude, close to the mass diffusion time, D/δ^2, where δ is the flame standoff and D is the diffusion coefficient. In this low-flow case, escaping fuel vapor from the flame-tip-sphere opening might be the dominant source of fuel vapor to create a combustible mixture for pulsation, between the two sources discussed previously in Section 3.1.

The pulsation frequency starts at 1.4 Hz, gradually decreases to 1 Hz, and is statistically constant in a 640 s to 1200 s period. The frequency further drops to 0.8 Hz before quenching at 1238 s. During this quasi-steady period, the pulsation amplitude increases with

time (Fig. 5(a)). Figure 6 presents the spread tracking of the flame tip1 in Fig. 5(a) in several selected time periods. At the start of a pulsating cycle, the flame tip position is set to zero. Flame tip position in the following frames of this cycle is compared to the starting frame to determine the distance the flame tip travels. The speed of the flame tip pulsation is slow in the beginning, reaches peak in the middle, and slows down when reaching the spreading limit. The solid line in Fig. 6 indicates the peak pulsation speed is around 25 cm/s, within the range of typical laminar premixed flame burning velocity. The tip shrinking is fast at the beginning but slows down approaching to the stagnation region. The tip stays at the starting position for a relatively long time get enough fuel vapor for the next pulse. There are no significant differences on the downstream pulsation speed in the beginning of the cycles. The total time for each cycle slightly increases during this quasi-steady period mainly due to the increase in the pulsation amplitude. Note that there is also variation from cycle to cycle so the trend on cycle frequency variation mentioned above is the statistical average.

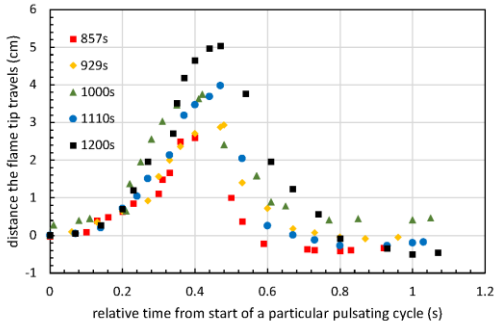

Fig. 6. Flame tip spread tracking of tip1 in Fig. 5 during selected pulsation cycles from Case #4. Relative distance and time compared to the starting frame is plotted.

Figure 7 shows the flame images of a representative pulsation cycle from Case #4, where the flame is close to quenching. In this example, the left and right tips in the images both pulsate. Figure 7(a) shows the asymmetry of flame tips before they start pulsating downstream. During downstream pulsating, the flame tip in Fig. 7(c) shows extended reaction zones at the near wake region of the spherical sample. The flame tip image in Fig. 7(c) shows a clear triple flame structure [19]. These are evidence that the flame tips are spreading into a premixed region. While flame tips are still spreading, part of the flame becomes dim before tip shrinking (Fig. 7(e)). After one cycle, the flame tip shrinks to a location further upstream (Fig. 7(h)).

Figure 8 shows the flame standoff distance tracking at the stagnation point and the conductive heat loss into the solid interior during the cyclic quenching period. The average standoff starts at 7 mm and gradually increases to 10 mm, in response to the variations in the conductive heat loss. This is a very large flame standoff distance for a solid fuel (inset flame image in Fig. 8), which is made possible in very low flow in microgravity. The oscillations in flame standoff distance, shown in the inset to Fig. 8 are attributed to the flow oscillation that is in turn caused by the large amplitude flame pulsations.

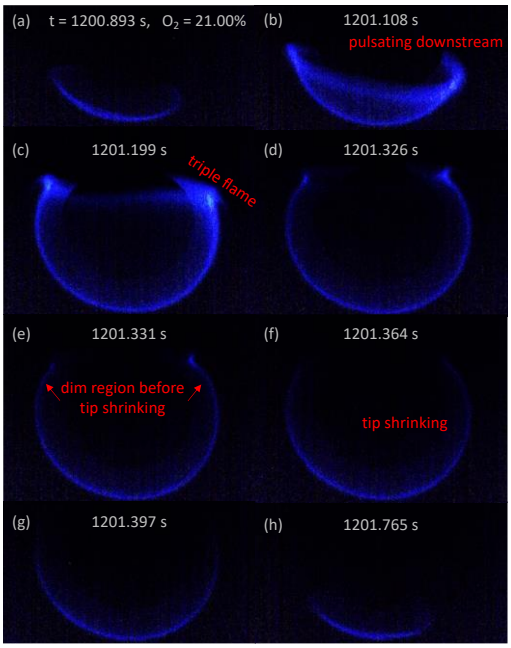

Fig. 7. One flame pulsation cycle in ultra-low-velocity flow and high oxygen environment (Case #4). Left tip corresponds to tip2 in Fig. 5.

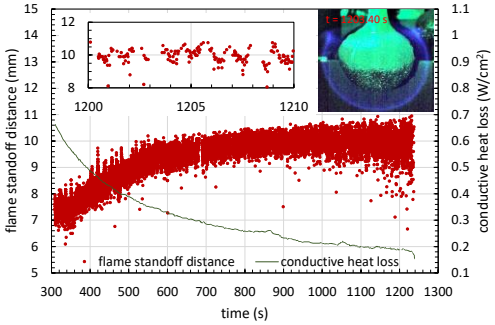

Fig. 8. Tracking of the stagnation-point flame standoff distance and conductive heat loss into the solid interior for Case #4. Legend and axes are the same for inset.

Readers are referred to the supplementary video S4 for a complete view of the cyclic flame pulsation process.

3.5 Side-stabilized and near-limit spinning flame

Case #5 has the highest flow velocity among the five cases (50 cm/s) and the sample is located at the duct exit so the long flame tip can freely expand outward without wall constriction. Figure 9 shows its flame profiles. Before local blowoff at the stagnation point, Fig. 9(a) shows an envelope flame with a very interesting structure. The flame tail spreads outward, but an inner weaker flame is also formed as indicated in the figure. This inner flame is connected to the downstream outer flame but extends backward and ends close to the solid surface. This inner flame is attributed to the recirculation zone behind the sphere (Re ~ 1300) where the oxygen recirculates back to the rear of the sphere and reacts with the fuel vapors that may otherwise escape to the ambient. In Case #2, the sphere is inside the duct for extinction, and the recirculation zone is reduced due to the squeeze of the flame by the duct wall. The inner flame in this case is a weaker diffusion flame judging from its faint color compared with that at the stagnation point. This is expected from the lower velocity of the recirculating flow. This type of enveloping diffusion flame may be unique only for blunt-shape solids that have a flow separation region.

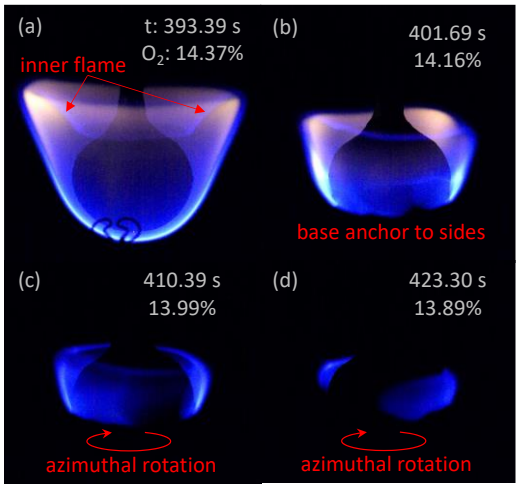

Fig. 9. Side-stabilized flame and azimuthal spinning after local blowoff in a high-flow blowoff case (Case #5).

Similar to Case #2, local blowoff occurs with a hole in the front stagnation region. The flame then stabilizes, and the flame base anchors at the shoulder of the sphere (Fig. 11(b)). The anchor flame base is indicated by the intense color due to high reactivity. In this test, the side-stabilized flame lasts for 40 s, around 35 s during which the flame is spinning. With continued oxygen depletion, the flame breaks into flamelets (Fig. 11(c) and (d)). The flamelet spins with frequencies ranging from 2 to 3.5 Hz. During spinning, the flamelets cover a shrinking surface area of the sphere due to oxygen depletion. With more and more area exposed, the solid surface cools down until the fuel vapor generated is not enough to sustain burning. This blowoff and flame spinning sequence is very dynamic (see supplementary video S5).

4. Summary and discussions

This is the first report on the experimental findings from a recent microgravity experiment aboard the International Space Station studying the burning of a 4-cm diameter PMMA sphere. One of the main objectives of the experiment is to study solid diffusion flame extinction processes. Using an oxygen depletion method at specified flow velocities, both the transient details of the low-flow quenching and high-flow blowoff processes are revealed.

Quenching starts with the flame tip shrinking toward the stagnation region. Extinction occurs when the shrinking flame at the forward stagnation point becomes too small. An early quasi-steady model over a thin solid with surface radiative heat loss has predicted this trend [21]. The present experiment, however, shows that this trend of steady shrinking flame is only true for the average flame. The actual quenching process is very dynamic involving flame tip local fluctuation and downstream cyclic pulsations all the way to the back of the sphere over many cycles. In pulsations, flame tip spreads into partially premixed mixture next to the hot solid surface. The mixture is created by leakage of fuel vapor from the opening between the flame tip and the solid surface and solid pyrolysis from the still hot solid after the flame tip cyclic shrinking. In low stretch flames, this opening is large, which enhances the importance of fuel leakage contribution to the cyclic pulsations. In a higher oxygen atmosphere (>21%) and ultra-low flow velocity (< 1 cm/s), pulsative motion can last for more than 15 minutes. These implications for spacecraft safety need to be explored further.

Blowoff starts with a hole opening at the stagnation region in front of the envelope diffusion flame. This is well known experimentally and studied in detail in [20]. An early quasistatic numerical model on thin solid also predicted the local blowoff of the stagnation flame and the possibility of side stabilized diffusion flame with increasing flow velocity or decreasing Damkohler number [22]. Again, experiments show that the extinction process is dynamic. Cyclic upstream pulsation and flame base retreat can proceed to the stabilization of the flame at the shoulder of the spherical sample. When the flame is weakened by reduced oxygen, flamelets form and azimuthally spin around the sphere. Other possible wake flame configurations have not been observed in the present setup possibly owing to the presence of the sample supporting rod.

Regarding the near-limit flame extinction dynamics: while cyclic flame movement are observed both in quenching and in blowoff, there is a profound difference between the two cases. The pulsating part is the flame tip in quenching and the flame base in blowoff. The stagnation region is the flame stabilization zone whereas tip is not. However, both

cases are coupled with the hot solid surface which supplies the fuel vapor for the flame to pulsate.

We note that blowoff and quench have been studied using a PMMA cylinder aligned with the flow[5, 20]. Using a large sphere, we have a better-defined stagnation shoulder, and wake flow zones. The multiple embedded thermocouples enable us to characterize the sample preheat levels. The low-velocity control also provides better resolved quenching limits.

Also, regarding the scale effect of the sample on quenching: low stretch flames can be established using large samples in higher velocity flows [6-8] or using smaller sample in lower velocity flow such as in the present work. Although both can achieve the same low flame stretch rate, the near-limit behavior can differ in the details. In large sample, flame breaks into flamelets, strips or holes before the quenching of the complete flame. The flamelets are of the dimension of diffusion length. In the present work using smaller sample, there is pulsative motion but no flamelet formation during the quenching process. So, the detailed quenching and blowoff process can be multi-dimensional in nature. They cannot be prescribed by the flow strain or flame stretch rate alone. An additional length scale may be required.

One final remark on the diffusion flame extinction criterion. Even in the one-dimensional description of diffusion flames, one may wonder whether a single Damkohler number can be sufficient to describe both blowoff and quenching limits. Both are extinction processes and the concept of limiting ratio of chemical vs. flow times seems applicable. However, quantifying the chemical reaction rate will need accurate flame temperature information. The actual flame temperature will be affected by heat loss, so additional non-dimensional heat loss parameter(s) will be required. We believe that quenching and blowoff are distinct flame extinction modes having different characteristics. Blowoff at high speed is due to short flow residence time in the flame stabilization zone. Blowoff can occur even at adiabatic flame temperature (i.e., no heat loss) as demonstrated in classical theory. So, although heat loss may modify the blowoff boundary, its effect is modest (ratio of heat loss to heat generation is small) and the flame temperature drop below the adiabatic value can be relatively small. On the other hand, at low stretch (low flow speed) with long flow residence time (or large flame standoff distance), aerodynamic quenching occurs when heat loss becomes a significant fraction of the total heat release of the flame. This causes substantial flame temperature reduction and leads to extinction. We have demonstrated in the GEL experiment not only the existence of the two extinction branches but also describe their different mechanisms and transient responses. In addition, the flame behaviors when the two extinction boundaries merge have been clarified.

Declaration of competing interest

The authors declare that they have no known competing financial interests or personal relationships that could have appeared to influence the work reported in this paper.

Acknowledgements

This research is funded by NASA under grant #80NSSC23M0035 from the Biological and Physical Sciences division of the NASA Science Mission Directorate. We like to thank the advice from Dennis Stocker, Dan Dietrich, and our International collaborators from Oleg Korobeinichev's group in Russian Academy of Sciences, Siberian Branch. The experiment hardware was built by, and operational support provided by, ZIN Technologies.

Supplementary material

There are five supplementary videos.

References

[1] F.E. Fendell, Ignition and extinction in combustion of initially unmixed reactants. J. Fluid Mech. 21 (1965) 281-303.

[2] A. Linan, The asymptotic structure of counterflow diffusion flames for large activation energies, Acta Astronaut. 1 (1974) 1007-1039.

[3] J.S. T'ien, Diffusion flame extinction at small stretch rate: the mechanisms of radiative loss, Combust. Flame 65 (1986) 31-34.

[4] X. Zhao, Y.-T.T. Liao, M.C. Johnston, J.S. T'ien, P.V. Ferkul, S.L. Olson, Concurrent flame growth, spread and quenching over composite fabric samples in low speed purely forced flow in microgravity, Proc. Combust. Inst. 36 (2017) 2971–2978.

[5] S.L. Olson, P.V. Ferkul, Microgravity flammability boundary for PMMA rods in axial stagnation flow: experimental results and energy balance analyses, Combust. Flame 180 (2017) 217-229.

[6] S.L. Olson, J.S. T'ien, Buoyant low-stretch diffusion flames beneath cylindrical PMMA samples, Combust. Flame 121 (2000) 439-452.

[7] B. Han, A.F. Ibarreta, C.J. Sung, J.S. T'ien, Experimental low stretch gaseous diffusion flames in buoyancy-induced flow fields, Proc. Combust. Inst. 30 (2005) 527-535.

[8] S. Tao, J. Fang, L. Zhao, J. Wang, R.S. Hassan, L. Yang, Burning characteristics of PMMA with varied stretch rates under stagnation-point diffusion flames, Combust. Flame 220 (2020) 63-72.

[9] O. Fujita, Solid combustion research in microgravity as a basis of fire safety in space, Proc. Combust. Inst. 35 (2015) 2487-2502.

[10] G.A. Ruff, D.L. Urban, M.D. Pedley, P.T. Johnson, Fire Safety, Chapter 27, Safety Design for Space Systems, (2009) 829-883

[11] P.V. Ferkul, available at < https://ntrs.nasa.gov/api/citations/20190030735/downloads/20190030735.pdf>
[12] W.Y. Chan, J.S. T'ien, An experiment on spontaneous flame oscillation prior to extinction, Combust Sci. Technol. 18 (1978) 139.
[13] D.L. Dietrich, H.D. Ross, Y. Shu, P. Chang, J.S. T'ien, Candle flames in non-buoyant atmospheres, Combust Sci. Technol. 156 (2000) 1-24.
[14] M.C. Johnston, *Growth and Extinction Limits: Ground Based Testing of Solid Fuel Combustion in Low Stretch Conditions in Support of Space Flight Experiments*, PhD thesis, Case Western Reserve University, Cleveland, Ohio, 2017.
[15] C. Li, J.S. T'ien, M.C. Johnston, S.L. Olson, P.V. Ferkul, Ignition of thermally thick blunt body PMMA samples using a heated wire, Fire Saf. J., 133 (2022)
[16] M. Endo, J.S. T'ien, P.V. Ferkul, S.L. Olson, M.C. Johnston, Flame growth around a spherical solid fuel in low speed forced flow in microgravity, Fire Technol. 56 (2020) 5–32.
[17] C. Wu, P. Sun, X. Wang, X. Huang, S. Wang, Flame extinction of spherical PMMA in microgravity: effect of fuel diameter and conduction, Microgravity Sci. Technol. 32 (2020) 1065-1075.
[18] T.A. Bolshova, I.E. Gerasimov, A.G. Shmakov, O.P. Korobeinichev, Combustion of spherical PMMA samples in still air simulated using a skeletal chemical kinetic mechanism, Fire Saf. J. 138 (2023)
[19] S.H. Chung, Stabilization, propagation and instability of tribrachial triple flames, Proc. Combust. Inst. 31 (2007) 877-892.
[20] S.L. Olson, P.V. Ferkul, J.W. Marcum. High-speed video analysis of flame oscillations along a PMMA rod after stagnation region blowoff, Proc. Combust. Inst. 37 (2019) 1555-1562.
[21] P.V. Ferkul, J.S. T'ien, A model of low-speed concurrent flow flame spread over a thin fuel, Combust. Sci. Tech 99 (1994) 345-370.
[22] C.H. Chen, J.S. T'ien, Diffusion flame stabilization at the leading edge of a fuel plate, Combust. Sci. Technol. 50 (1986) 283.